IB Physics Extended Essay

Maximizing the energy production of a fixed-position solar panel

What is the optimal tilt angle of a fixed-position polycrystalline photovoltaic solar panel located in Geneva, Switzerland with respect to maximum annual energy generation?

Figure 1. Solar panel array located in the Alps above Disentis, Switzerland (Bond)

Word Count: [3981]

Candidate personal code: gnm174

Date: 07/01/2020

Table of Contents

I. INTRODUCTION

A. Motivation for the investigation

Solar power—promising a steady supply of clean, renewable energy while emitting no greenhouse gases—is an increasingly popular and valuable asset in the fight against climate change. As its use becomes increasingly widespread, solar faces key challenges: energy storage has not yet caught up to developments in solar tech, leading to problems like “the duck curve”, where solar production capacity declines right as peak demand is reached (Office of Energy Efficiency & Renewable Energy, 2017). Furthermore, commercial solar panels are generally less efficient, capturing only a small fraction of the sun’s energy (~18%) (ISE, 2019).

Strategic positioning of fixed-position (non-tracking) solar panels can improve energy production, mitigating efficiency shortcomings. This investigation therefore seeks to maximize the energy production of a fixed-position solar panel over the course of a year for Geneva, Switzerland.

Similar optimization case studies have been carried out worldwide, in diverse locales including Ontario, Canada (Rowlands, Kemery, & Beausoleil-Morrison, 2011); Pristina, Kosovo (Berisha, Zeqiri, & Meha, 2018); and Brisbane, Australia (Yan, Saha, Meredith, & Goodwin, 2013). However, these studies’ findings may not necessarily pertain to Switzerland’s particular geographic and climatic features. Mountains cover 70% of Switzerland’s surface area, (Federal Office of Topology, 2017) offering both enormous advantages—harnessing hydroelectric power for solar power storage, and challenges—using solar arrays in regions with extensive snowfall or lingering cloud cover during winter.

B. Photovoltaic solar cells

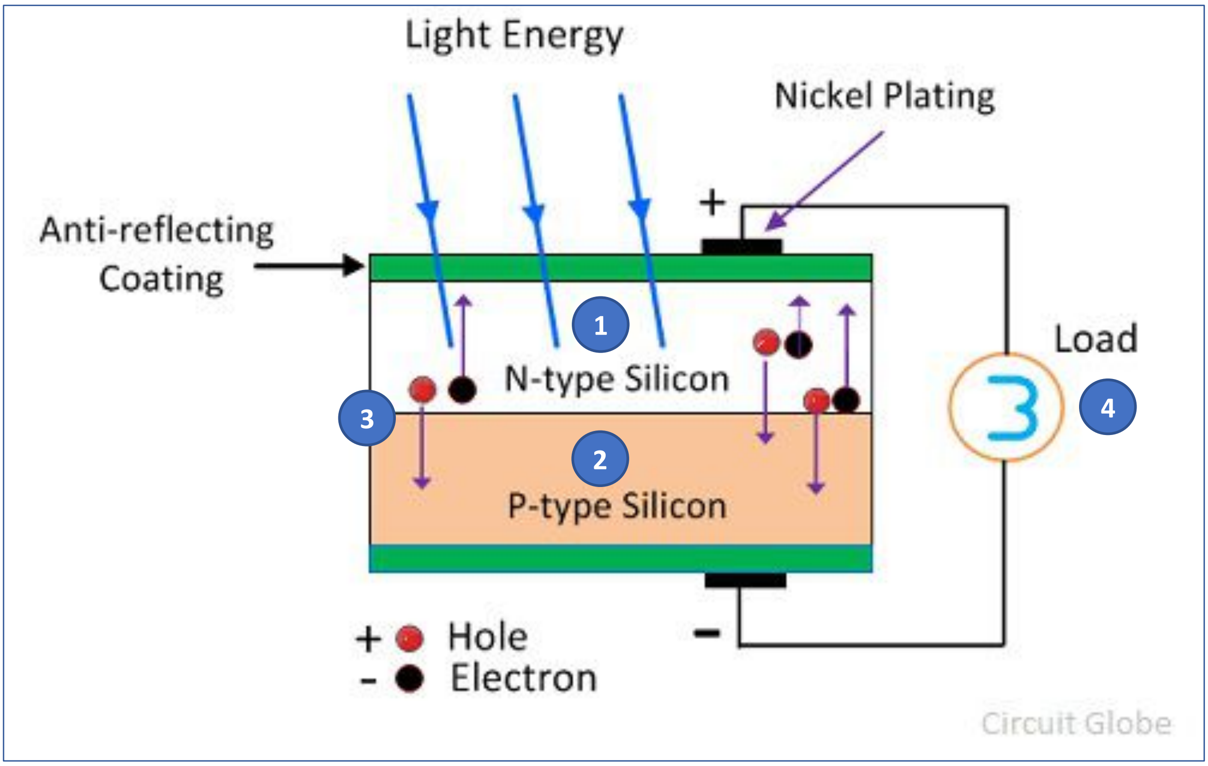

Figure 2. Diagram of a photovoltaic cell. (CircuitGlobe)

Typical photovoltaic (PV) cells (Figure 2) such as the one considered in this investigation are composed of a positively-charged N-type 'phosphorus-doped' silicon layer (1), on top of a negatively-charged P-type 'boron-doped' silicon layer (2), with an electric field in the middle called an 'N-P' junction (3). The N-type layer contains an excess of electrons, while the P-type layer contains an excess of 'holes'—spaces absent of electrons. When a photon collides with the N-type layer, it emits an electron through the photoelectric effect. This electron is acted upon by the N-P junction electric field, preventing it from returning to its atom, and passing it from the N-layer to P-layer, creating a flow of electrons and therefore current in the cell when connected to a source of electrical load (4). A string of individual solar cells linked together compose a solar module; multiple modules together form a solar array. (CircuitGlobe, 2018)

C. Solar angles

Solar collectors produce the highest power output when positioned perpendicular to the sun's rays. For fixed-position panels, it is vital to find a position that minimizes the average offset from the perpendicular over an interval of time (e.g., a year).

Two angles define the positioning of a fixed-position solar panel: **Azimuth γ** is the bearing of a panel (clockwise) from true South in degrees (Figure 3); **Slope β** (tilt) is the angle subtended between the panel and the horizontal plane.

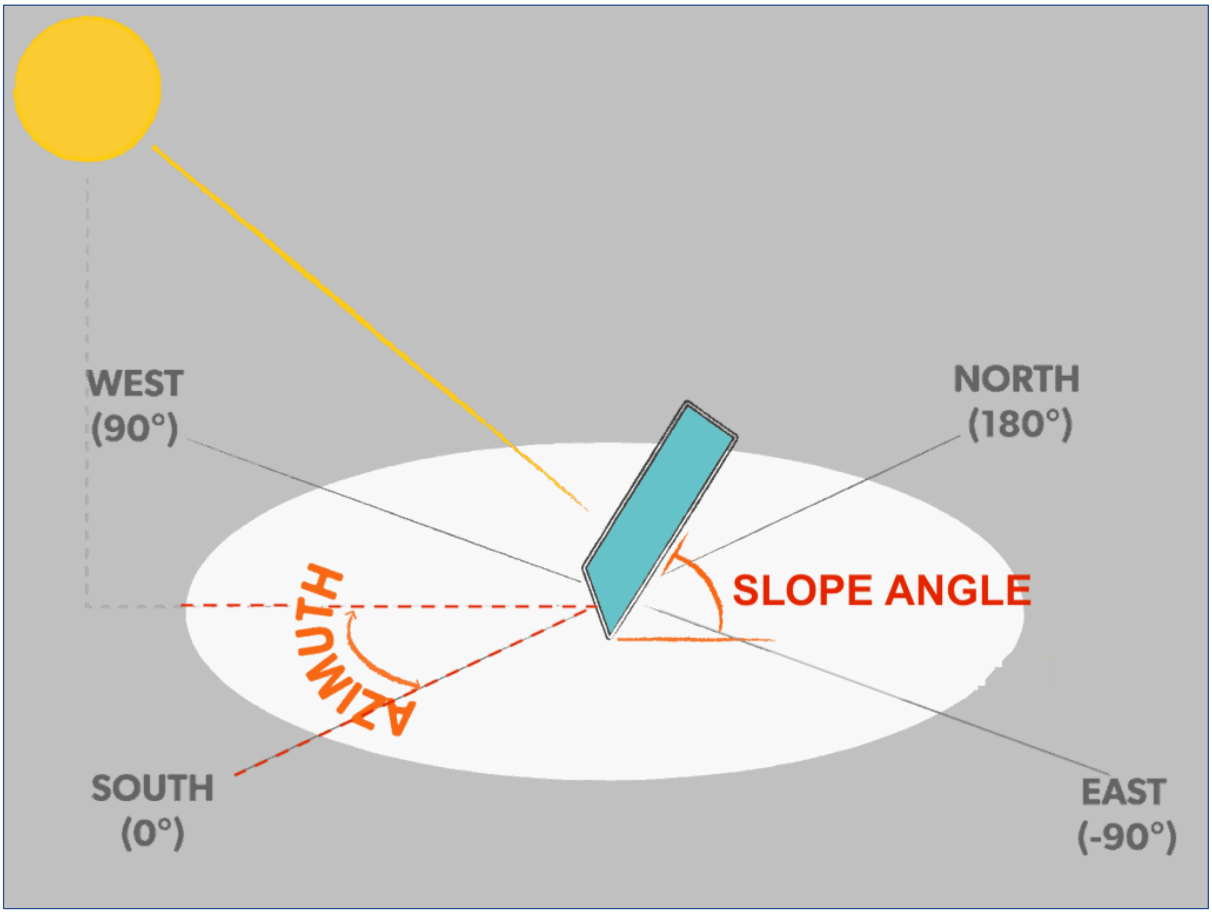

Figure 3. Solar azimuth and slope angles (Allen, 2018)

In this study slope angle will be optimized for output energy production. Azimuth was not considered, because energy output is usually maximized when panels point to true South in the northern hemisphere (Duffie & Beckman, p. 24).

The angle of incidence (AOI, θ) is defined as the angle between the normal to the solar panel, and the incoming solar radiation, and can be calculated using the geometric relation from literature (Duffie & Beckman, pp. 34-36) below, with declination angle δ, latitude ϕ, slope β, azimuth γ, and hour angle ω calculated in Excel as described in section II-B-6.

$$\begin{aligned} \cos\theta = {} & \sin\delta \sin\phi \cos\beta - \sin\delta \cos\phi \sin\beta \cos\omega + \cos\delta \cos\phi \cos\beta \cos\omega \\ & + \cos\delta \sin\phi \sin\beta \cos\gamma \cos\omega + \cos\delta \sin\beta \sin\gamma \sin\omega \end{aligned} \quad (1)$$

D. Research question

This extended essay examines the question: “What is the optimal slope angle of a fixed-position polycrystalline photovoltaic solar panel located in Geneva, Switzerland to maximize annual energy generation?”

The generally accepted rule is that the optimum slope angle for a solar panel is roughly equal to the latitude where it is located (Benghanem, 2011), with optimum semi-annual adjustments of ± 15° from the latitude during the winter and summer months, respectively (Elminir, et al., 2006).

E. Literature survey

Several similar case studies have been conducted around the world, the majority arriving at the aforementioned relationship between location latitude ϕ and optimum annual panel slope β_{opt}:

Location	**Latitude**	**Optimum slope angle**	**Reference**
Ankara, Turkey	$\phi = 24.5°N$	$\beta_{opt} = 23.5°S$	(Bakirci, 2012)
Madinah, Saudi Arabia	$\phi = 24.5°N$	$\beta_{opt} = 23.5°S$	(Benghanem, 2011).
Tabass, Iran	$\phi = 33.4°N$	$\beta_{opt} = 32°S$	(Mohammadi, Mostafaeipour, & Khorasanizadeh, 2014)
Brisbane, Australia	$\phi = 27.5°S$	$\beta_{opt} = 26°N$	(Yan, Saha, Meredith, & Goodwin, 2013)
Helwan, Egypt	$\phi = 29.8°N$	“approximately equal to site’s latitude”	(Elminir, et al., 2006)

Maleki et al. summarize additional locations in Table 10 of their paper (2017).

Many other case studies (see above) seek exclusively to maximize radiation received on a surface (irradiance), without regard to maximizing energy output. A key difference in the approach taken in this investigation is that the variety of solar panel is known and therefore output energy can be estimated, based on known panel-specific qualities.

F. Investigation methodology

This investigation is in three parts, detailed in Section II of this essay:

II A - Experimental data collection: A laboratory experiment to establish a formula for the efficiency of a polycrystalline photovoltaic (PV) solar panel as a function of incoming radiation angle of incidence (AOI).

II B - Secondary database and insolation model: An estimate of the total solar radiation received on a PV panel tilted at a given slope angle in Geneva, Switzerland, based on secondary data from MétéoSuisse; then an estimate of energy produced over a year by combining the incident irradiance with experimental panel efficiency function (II A).

II C – Optimization, results and analysis: Repeating the process to estimate output energy for panel slopes from 0°-90° to find an optimum panel angle for maximizing annual energy generation; and determining optimum periodicity of fixed-position solar panel tilt adjustment.

II. INVESTIGATION

A. Experimental Data Collection

1. Aim and Experimental Hypothesis

The aim of this experiment was to investigate the effect of the angle of incidence (AOI, θ) of incoming light from a projector (representing solar radiation) on the efficiency of a polycrystalline photovoltaic panel.

The efficiency (%) of the test solar panel is not directly measurable, so calculations were performed to establish it. Panel efficiency (η_{panel}) can be expressed as:

$$\eta_{panel} = \frac{I_{out}}{I_{in}} \qquad (2)$$

where I_{out} is the **output** intensity—power generated by the panel per unit area (W·m^{-2})—and I_{in} is the **input** intensity of the light incident on the panel surface (in W·m^{-2}). I_{out} was the variable measured in this experiment; I_{in} required further calculations.

I_{in} is the product of the projector light intensity $I_{proj.}$ and the cosine of the AOI, $cos\ \theta$, according to Lambert's cosine law (Weik, 2001):

$$I_{in} = I_{proj.} \times cos\ \theta \qquad (3)$$

The $cos\ \theta$ term is included because as the AOI increases, and the incident light arrives at increasingly glancing angles, the catchment surface area 'visible' to $I_{proj.}$ (h in Figure 4) will decrease in a $cos\ \theta$ relationship.

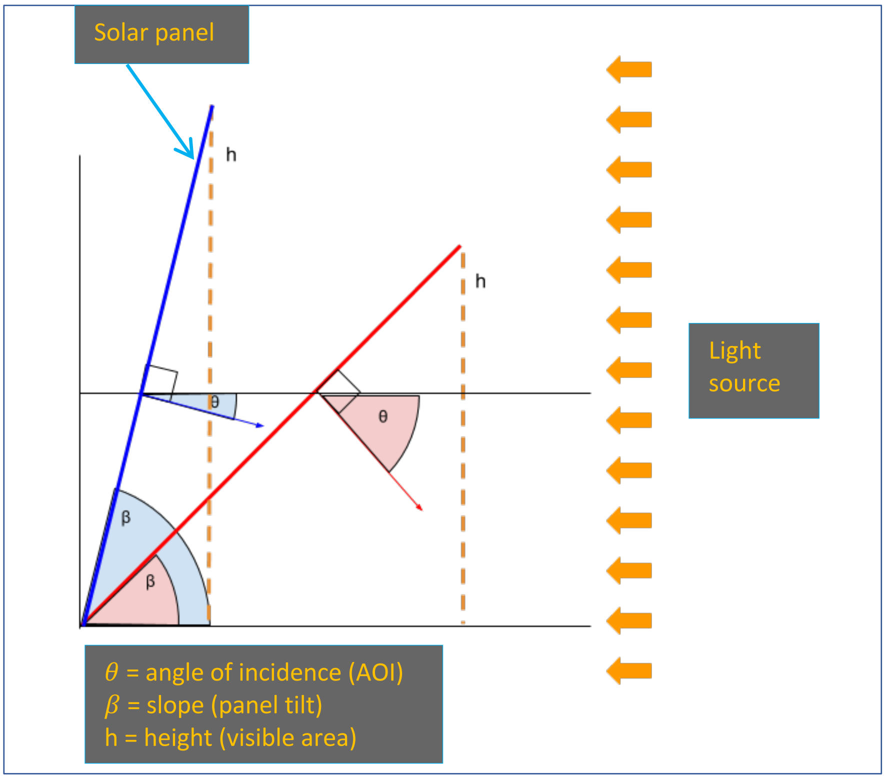

Figure 4. Illustration of reduced visible area (h) resulting from increased AOI (θ)

After accounting for Lambert's Cosine Law the remaining efficiency should be a function of the reflected light % at each angle and factors specific to the PV cell. The silicon power generation characteristics are beyond the scope of this investigation; nevertheless, it can be hypothesized that the reflected light should cause the majority of the loss in efficiency as the angle becomes more glancing, according to Fresnel's reflectance equations, as discussed later.

a) Finding the projector light intensity

To find incoming light intensity (W·m^{-2}) from the projector ($I_{proj.}$), the illuminance was measured at a distance of 0.75 m from the projector lens using a luxmeter and found to be 10'080 lux. Since the panel was actually positioned 0.42 m away from the lens, the corresponding intensity was found as follows:

$$lux(E_v) \times distance(D)^2 = candela(I_v) \quad (4)$$

$$10080 \times (0.75)^2 = 5670\ cd \quad (5)$$

The illuminance E_v was first converted to candela I_V (Eq. 4, 5) given a distance D of 0.75 m, giving $I_v = 5670$ cd; that candela was converted back to illuminance E_v (Eq. 5, 6) at a new distance D of 0.42 m:

$$\frac{I_v}{D^2} = E_v \tag{6}$$

$$\frac{5670}{(0.42)^2} = 32'143\ lux \tag{7}$$

Thus, at a distance of 0.42 m the projector provides an illuminance of 32’143 lux. Converting this to intensity (W·m^{-2}) entails combining the equations for luminous efficiency ($\eta_{bulb} = \frac{lumens}{Watt} = \frac{lm}{W}$) and lux ($lux = \frac{lumens}{m^2} = \frac{lm}{m^2}$):

$$\frac{lm}{m^2} \div \frac{lm}{W} = \frac{lm}{m^2} \times \frac{W}{lm} = \frac{W}{m^2} = Intensity\ (W \cdot m^{-2}) \tag{8}$$

The projector’s halogen bulb is rated at 6000 lumens with a power draw of 150 W (OSRAM, 2007), giving a luminous efficiency of: $\eta_{bulb} = \frac{lm}{W} = \frac{6000}{150}$. To find the intensity at 0.42 m:

$$\frac{lux\ (lm/m^2)}{\eta_{bulb}\ (lm/W)} = \frac{10080}{\left(\frac{6000}{150}\right)} = \frac{32143}{40} = 804W\ m^{-2} \tag{9}$$

Hence our panel had an intensity from the projector ($I_{proj.}$) of 804 watts per meter squared.

This step contains a significant margin of uncertainty: while the halogen bulb inside the projector radiated light isotropically, the projector lens acted as a collimator, narrowing the beam, and potentially interfering with the luxmeter measurement used for finding $I_{proj.}$.

b) Adjusted incident intensity

To account for the diminishing ‘visible’ area effect (Lambert’s cosine law, mentioned earlier), the incident panel intensity (I_{in}) will equal the projector intensity times the proportion ($cos\ \theta$) that will be visible at any given AOI (θ):

$$I_{in} = I_{proj.} \times \cos\theta \tag{10}$$

$$\therefore\ I_{in} = 804 \times cos\ \theta \tag{11}$$

2. Variables

a) *Independent variable*

The **angle of incidence** was varied in a range of 0° to 90° on the horizontal plane in 5° increments. A quarter-circle was drawn around the center of rotation, serving as a protractor; a ruler extending from the PV module pointed to the angle, reducing the uncertainty to $\pm 0.5°$.

b) *Dependent variable*

Power output in Watts (W): calculated by multiplying potential difference (V) and current (A) readings across a source of load in the PV module circuit, both measured using a LabQuest datalogger accurate to 0.01 V and 1 mA respectively, although the values fluctuated during measurements, so the uncertainty was determined to be ±0.05 V and ±5 mA, hence ±0.25 mW.

c) *Controlled & uncontrolled variables*

The following *controlled* variables were kept constant:

- **Background light**, by shutting blinds and darkening lab
- **Temperature and humidity**, by conducting all trials in one sitting
- **Projector irradiance**, by keeping the projector at 0.42 m for all trials

The following *uncontrolled* variables possibly differed between trials:

- **Radiation reflected** off nearby objects
- **Radiation diffused** in atmosphere

3. Methodology

a) *Apparatus & setup*

The apparatus comprised a slide projector projecting a focused beam onto a 15x20 cm polycrystalline PV module, with an ammeter, voltmeter, and a luxmeter on a swiveling arm directed at the panel to measure reflected light (Figure 5). The data collection circuit was set up as shown in Figure 6.

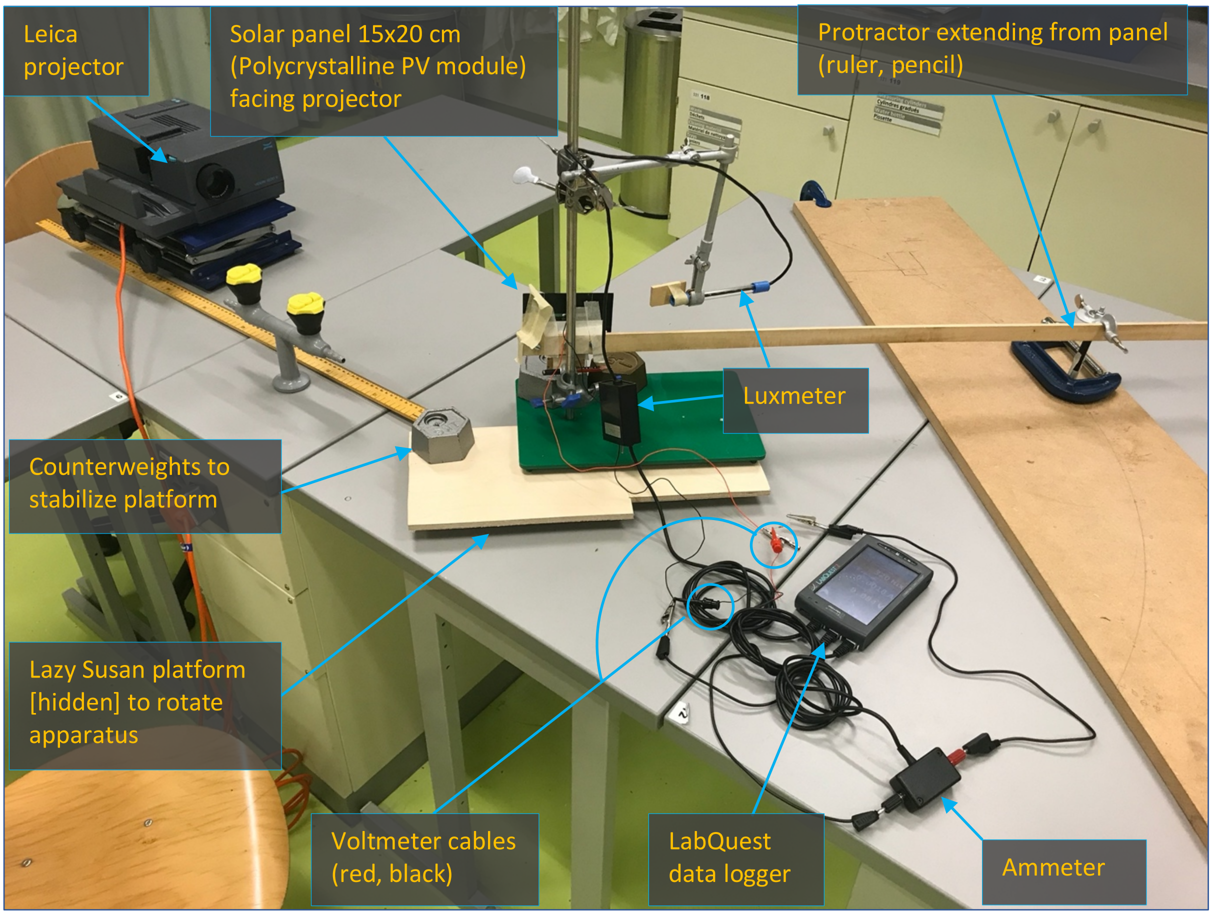

Figure 5. Overview of experimental setup

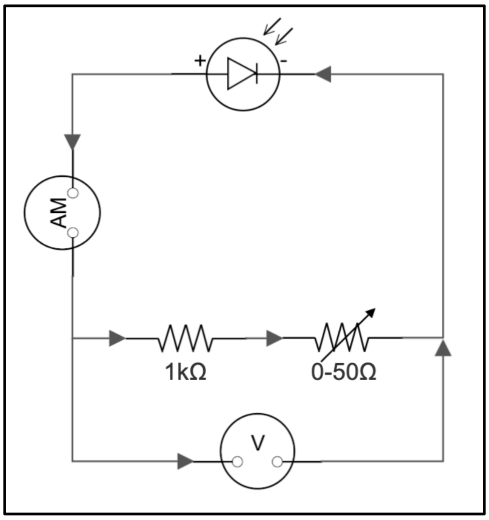

Figure 6. Diagram for PV-measurement circuit, created with circuit-diagram.org

b) Risk Assessment

The experiment apparatus and method were determined to pose negligible safety concern or environmental harm: voltages and currents conform to class 3 of IEC standard 60950-1, a "SELV (Safety Extra Low Voltage) supply circuit", meaning it inherently protects against shocks, given that it is incapable of generating dangerous voltages (IEC IECEE, 2005). To minimize fire risk, the projector was turned off when not in use.

c) Method

For the apparatus and circuit (Figures 5, 6), a 1 kiloohm (kΩ) resistor was used as a source of electrical load, as it appeared to maximize output power in preliminary testing with the variable resistor. The ruler arm was moved in 5° increments, with corresponding AOI, voltage, and current recorded; the luxmeter moved in an arc pointing at the panel, recording the luminosity of the reflected light.

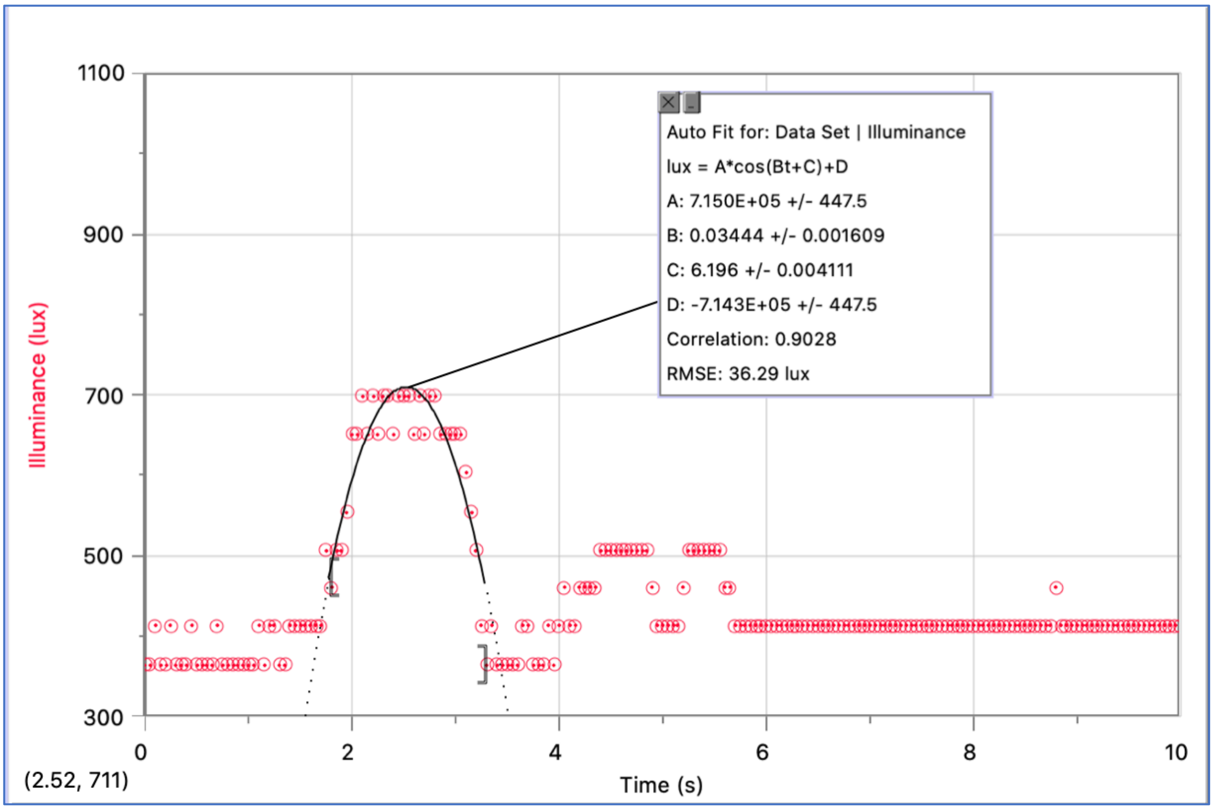

Figure 7. Finding the maximum reflected light from illuminance vs. time graph (θ=35°)

The maximum reflected light illuminance was then found by graphing illuminance vs. time for each trial and interval (Figure 7) and finding the maximum lux value recorded, to determine the extent to which lost light results from reflection, considering solar modules can make use of anti-reflective coatings.

4. Experimental results

a) Raw data

Table 1
Raw power output values from solar panel

		Trial 1			Trial 2			Trial 3		
Slope angle β (deg.)	**AOI θ (deg.)**	**Current (A)**	**Potential Difference (V)**	**Power (W)**	**Current (A)**	**Potential Difference (V)**	**Power (W)**	**Current (A)**	**Potential Difference (V)**	**Power (W)**
90	**0**	0.153	5.24	0.802	0.153	5.032	0.770	0.159	5.266	0.837
85	**5**	0.150	5.03	0.755	0.156	5.281	0.824	0.150	4.876	0.731
80	**10**	0.153	5.11	0.782	0.147	4.971	0.731	0.153	5.114	0.782
75	**15**	0.153	5.08	0.776	0.153	5.101	0.780	0.153	5.101	0.780
70	**20**	0.141	4.60	0.649	0.141	4.741	0.668	0.147	4.822	0.709
65	**25**	0.144	4.71	0.679	0.138	4.616	0.637	0.144	4.601	0.663
60	**30**	0.126	4.22	0.532	0.135	4.501	0.608	0.126	4.260	0.537
55	**35**	0.123	4.14	0.509	0.123	4.029	0.496	0.126	4.220	0.532
50	**40**	0.114	3.56	0.405	0.114	3.822	0.436	0.111	3.685	0.409
45	**45**	0.108	3.54	0.382	0.111	3.565	0.396	0.108	3.477	0.376
40	**50**	0.093	3.09	0.287	0.099	3.163	0.313	0.093	3.053	0.284
35	**55**	0.081	2.71	0.220	0.081	2.719	0.220	0.084	2.830	0.238
30	**60**	0.072	2.31	0.167	0.075	2.381	0.179	0.069	2.187	0.151
25	**65**	0.048	1.86	0.089	0.054	1.845	0.100	0.054	1.866	0.101
20	**70**	0.039	1.37	0.053	0.039	1.328	0.052	0.039	1.353	0.053
15	**75**	0.024	0.85	0.020	0.027	0.878	0.024	0.024	0.788	0.019
10	**80**	0.003	0.41	0.001	0.009	0.403	0.004	0.009	0.414	0.004
5	**85**	0.000	0.10	0.000	0.003	0.091	0.000	0.000	0.087	0.000
0	**90**	0.000	0.04	0.000	0.000	0.046	0.000	0.000	0.045	0.000

b) Processed data

Table 2
Processed power output values from solar panel and efficiency calculation

AOI (°)	Average			Surface intensity out (W/m2)	Surface intensity in (W/m2)	Efficiency (%)
	Current (A)	Potential Difference (V)	Average power out (W)			
0	0.155	5.179	0.803	26.76	804	0.0333
5	0.152	5.064	0.770	25.66	801	0.0320
10	0.151	5.066	0.765	25.50	792	0.0322
15	0.153	5.092	0.779	25.97	777	0.0334
20	0.143	4.722	0.675	22.51	756	0.0298
25	0.142	4.643	0.659	21.98	729	0.0302
30	0.129	4.327	0.558	18.61	696	0.0267
35	0.124	4.130	0.512	17.07	659	0.0259
40	0.113	3.688	0.417	13.89	616	0.0226
45	0.109	3.526	0.384	12.81	569	0.0225
50	0.095	3.102	0.295	9.82	517	0.0190
55	0.082	2.754	0.226	7.53	461	0.0163
60	0.072	2.294	0.165	5.50	402	0.0137
65	0.052	1.855	0.096	3.22	340	0.0095
70	0.039	1.349	0.053	1.75	275	0.0064
75	0.025	0.840	0.021	0.70	208	0.0034
80	0.007	0.410	0.003	0.10	140	0.0007
85	0.001	0.092	0.000	0.00	70	0.0000
90	0.000	0.045	0.000	0.00	0	0.0000

Example calculation of efficiency %, where AOI=35°:

$$I_{out}\ (W \cdot m^{-2}) = \frac{P_{out,avg.}\ (W)}{A\ (m^2)} \tag{12}$$

$$\therefore I_{out} = \frac{0.512}{0.015 \times 0.020} = 17.07\ W \cdot m^{-2} \tag{13}$$

Calculating the input intensity using Equation 11:

$$I_{in} = 804 \times \cos\theta \qquad \text{Eq. 11}$$

$$\therefore\ I_{in} = 804 \times cos\,35° = 659\ \ W \cdot m^{-2} \tag{14}$$

Allows the panel efficiency η_{panel} to be found using Equation 2:

$$\eta_{panel} = \frac{I_{out}}{I_{in}} = \frac{17.07}{659} = 0.0259 = 2.59\% \tag{15}$$

5. Converting panel output power to efficiency conversion coefficient

The efficiency values for each AOI can be plotted in LoggerPro (Figure 8).

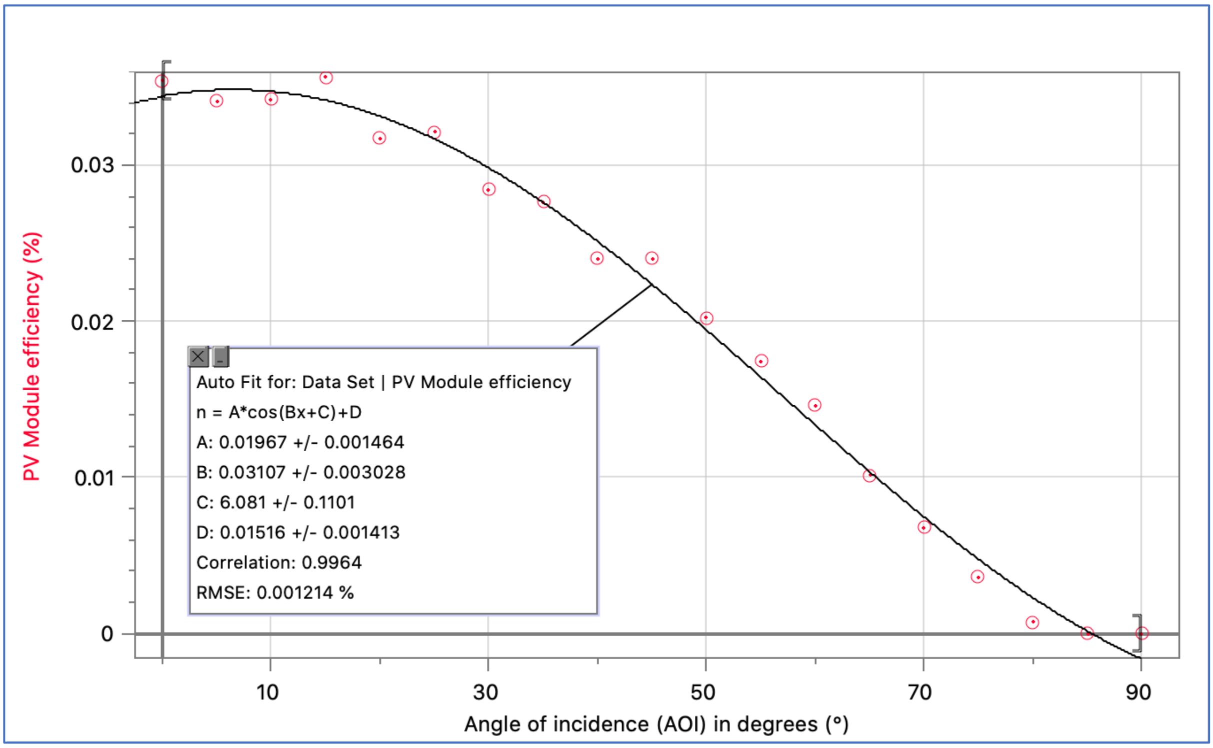

Figure 8. PV module efficiency (%) vs. Angle of incidence (°)

A cos-squared regression line is applied, assuming the following: Voltage and current should each have $cos\ \theta$ relationship with θ, hence power and output intensity have a $cos^2\ \theta$ relationship. Input intensity has a $cos\ \theta$ relationship. Therefore, the efficiency ($\frac{cos^2\ \theta}{cos\ \theta} = cos\ \theta$) should have a $cos\ \theta$ relationship with θ, with a domain of $0° \leq$ AOI (θ) $< 90°$ to prevent negative efficiency values, and outputting a value for efficiency such that:

$$P_{out} = P_{in} \times \eta \quad (16)$$

This is a simplistic interpretation of panel efficiency; many other factors come into play, including light wavelength, reflection off the panel, panel temperature (Solar technologies office, 2013). For the latter, a 1 °C increase in solar cell temperature would result in an efficiency decrease of 0.45%--which can rapidly compound on hot summer days, where black-colored panels are capable of reaching over 65 °C (Solar Calculator, 2015).

The parameters found using LoggerPro's best fit cos θ trendline yielded the following equation for efficiency as a function of the AOI:

$$\eta_{panel} = 0.01967 \times \cos(0.03107 \times x + 6.081) + 0.01516 \qquad (17)$$

The maximum reflected light from the panel at each AOI was also examined, to determine its effect on efficiency.

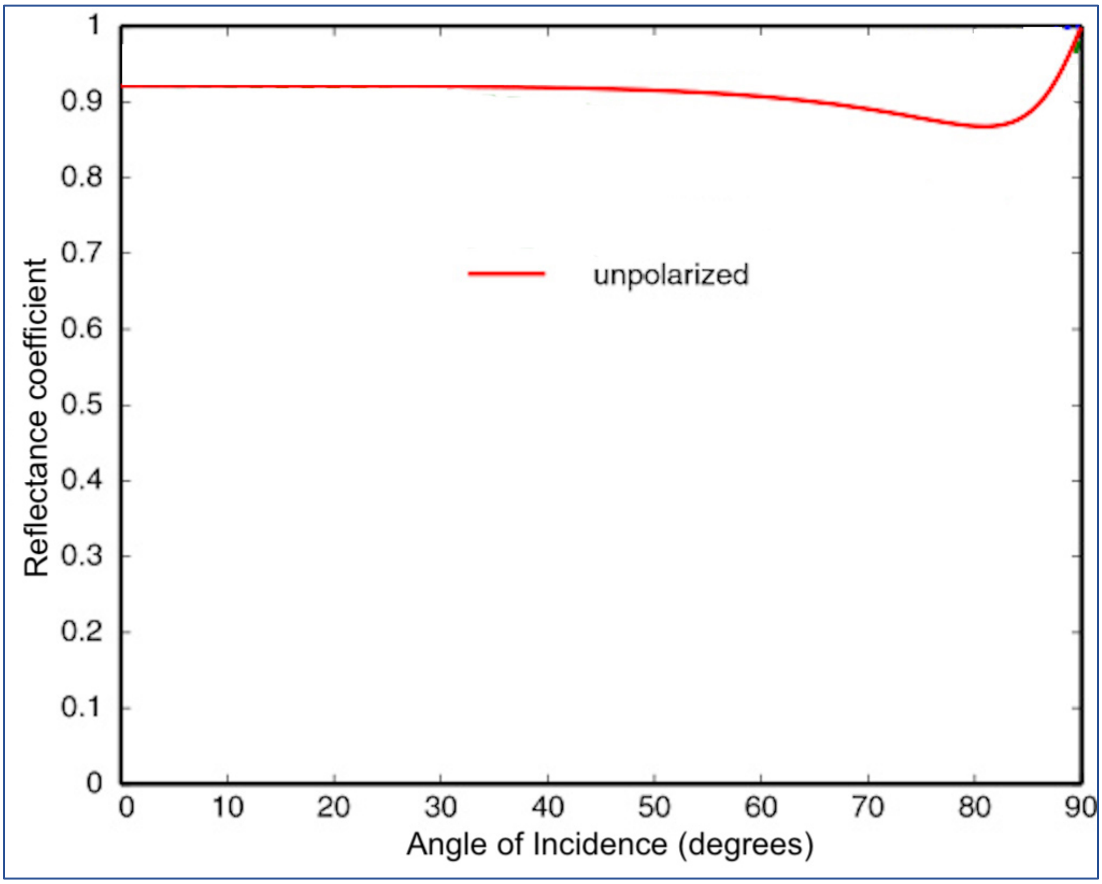

Figure 9. Reflection coefficient vs. Angle of Incidence for example glass-like material via (Westin, 2011).

Figure 9 presents an example relationship between the percentage of reflected unpolarized projector light and the AOI (or 'angle from normal'), in accordance with Fresnel's equations of reflectance (Westin, 2011). One can observe a local minimum point of reflectance, a plateau around 0°, and a convergence to complete reflectance (1.0) at 90°.

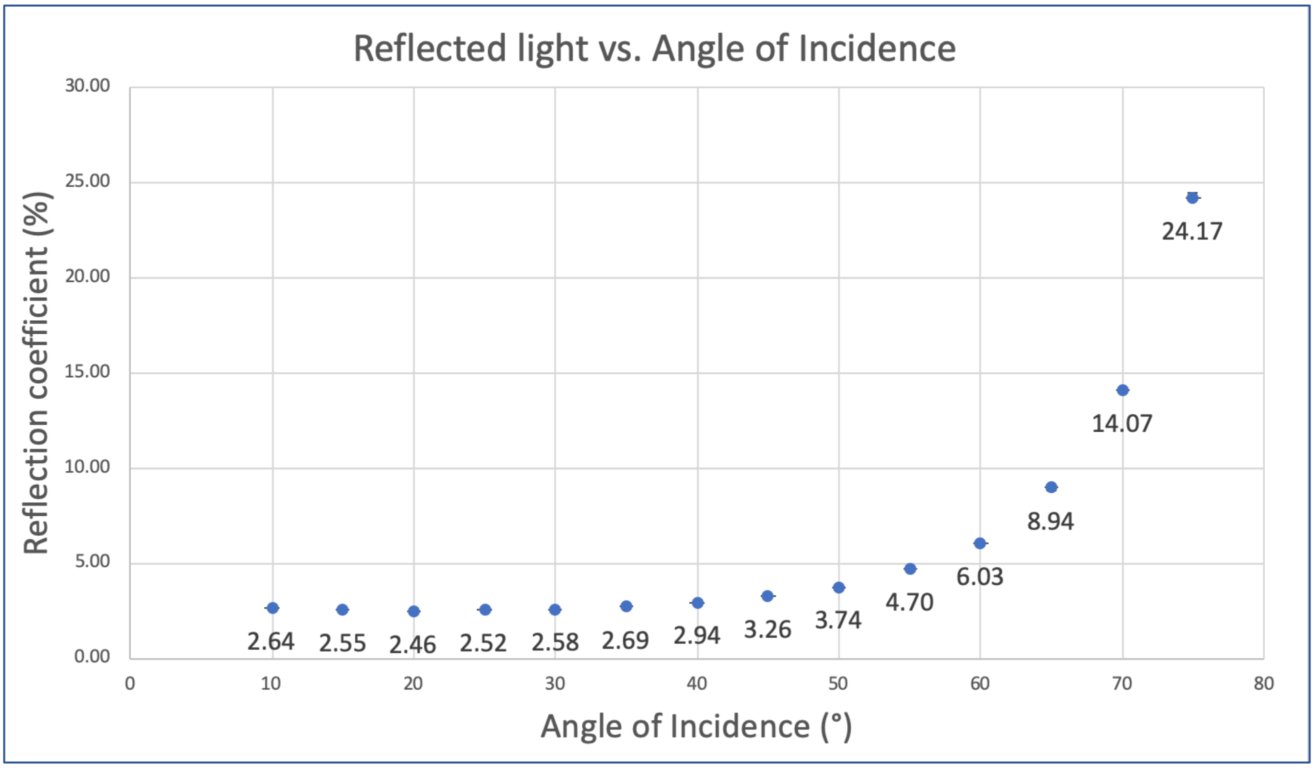

Figure 10. Experimental reflection coefficient vs. angle of incidence for solar panel

Several key features from Figure 9 are present in our experimental findings (Figure 10): a local minimum reflectivity at ~20°; a slight increase in reflectivity around 10 and 15° (data from before 10° was discarded due to the luxmeter blocking the projector); an exponential trend from 40°-75° (after 75° data was discarded, because the luxmeter would register light coming straight from the projector, not just the reflected light).

This demonstrates an advantage of experimentally finding efficiency as a function of AOI: unlike most studies listed in the literature survey, this approach accounts for the degree of reflection.

B. Secondary database and insolation model

1. Aim and overview of methods

The aim of this section is to model the total annual radiation energy incident on a panel at a given slope angle, located in Geneva, Switzerland, and from that, estimate the total annual energy output. This involved several steps:

- Collection of MétéoSuisse historical data for irradiation on a horizontal surface;
- Conversion of MétéoSuisse horizontal irradiation into tilted panel irradiation using the Liu & Jordan isotropic model to find hourly tilted irradiation;
- Conversion of hourly irradiance on the tilted panel surface to hourly output energy, using efficiency formula derived in Section IIA;
- Integration of output energy over the typical meteorological year to find total annual output energy.

2. Solar radiation terms

This investigation uses the following solar radiation terms: (The National Renewable Energy Laboratory (NREL), 2019)

- **Intensity, Power density** – Rate at which energy arrives on a specific area of surface ($W \cdot m^{-2}$)
- **Irradiance, Insolation, Irradiation** – Rate at which *solar* energy arrives on a specific area of surface ($W \cdot m^{-2}$)

3. Hourly global irradiance on a horizontal surface

Model calculations were based on MétéoSuisse historical irradiation data for Cointrin, Geneva, for a "typical meteorological year" (a representative sample from 10 years' data).

The total irradiance on a horizontal surface (global irradiance, I_H) is measured by a pyranometer directed straight up in an unsheltered area (Figure 11, #3).

Figure 11. Radiometric station in Ghardaïa city, Algeria (Rezrazi, Laidi, & Hanini)

I_H can also be expressed as the sum of its components:

$$I_H = I_b + I_d \quad (18)$$

where I_b is the horizontal "beam" irradiance, and I_d is the horizontal "diffuse" irradiance. Beam radiation refers to solar radiation before it has been scattered by the atmosphere, as if pointing a pyrheliometer (#5) directly at the sun and blocking all other sky. Diffuse radiation is light received from atmospheric scattering of solar radiation, found by blocking the sun in the pyranometer's line of sight (#2) using a shading ball (#1), measuring the irradiance from the sky/atmosphere, excluding beam radiation. This explains the complementary nature of diffuse and beam horizontal irradiance (equation 18).

The MétéoSuisse database comprises global and diffuse horizontal irradiation data, a sample of which is provided in Table 3. Beam radiation is calculated by rearranging equation 18:

$$I_b = I_H - I_d \quad (19)$$

Table 3
Sample horizontal global, diffuse, beam irradiance data (MétéoSuisse)

Date + time	I_H (W·m^{-2})	I_d (W·m^{-2})	(Calculated) I_b (W·m^{-2})
1/1/15 08:00	35	34	1
1/1/15 09:00	80	78	2
1/1/15 10:00	104	103	1
1/1/15 11:00	213	171	42
1/1/15 12:00	267	158	109
1/1/15 13:00	257	114	143
1/1/15 14:00	159	93	66
1/1/15 15:00	66	33	33

Given that raw irradiance data is given to the nearest $\mathrm{W{\cdot}m^{-2}}$, future calculations retain the same number of significant figures. Furthermore, MétéoSuisse provides 'plausibility' and 'modification' information for their data (MétéoSuisse, 2015). Tables 4 and 5 provide a plausibility status summary for the 10 years of data composing the typical meteorological year.

Table 4
***Diffuse** irradiance plausibility information from 2010-2019 MétéoSuisse data*

Plausibility status code	Status code definition	Number of occurrences in MétéoSuisse I_d data
0	No change to data	79559
128	Data missing, replaced with averaged value	13
-	Status unknown	751
	Grand Total	80323

Table 5
***Global** irradiance plausibility information from 2010-2019 MétéoSuisse data*

Plausibility status code	Status code definition	Number of occurrences in MétéoSuisse I_H data
0	No change to data	79254
128	Value averaged from incomplete data	5
256	Value averaged from uncertain data	24
1024	Value averaged from highly unusual/unlikely data	10
2048	Value averaged from highly unlikely data from same station	151
2304	Value averaged from uncertain data AND from highly unlikely data from same station (2048+256)	50
-	Status unknown	1
	Grand Total	79495

In both summary tables, the overwhelming majority (99.0%, 99.7%) of values had a plausibility code of 0: no modification or irregularity. 751 diffuse irradiation values had an unreliable status (0.9%), as did 242 global values (0.3%). From this, the data appears highly reliable, although some degree of uncertainty must be assumed for a decade's worth of data, despite not being easily quantifiable.

4. Estimating radiation incident on a tilted surface: Liu & Jordan Isotropic model

Given data for the global, diffuse, and direct horizontal irradiance, the next step was estimating *tilted* irradiance I_t using Liu & Jordan's isotropic sky model. In this model, irradiance on a tilted surface is split into three components (Eq. 20): tilted beam radiation I_{bt}, tilted diffuse radiation I_{dt}, reflected radiation I_r (Maleki, Hizam, & Gomes, p. 11).

$$I_t = I_{bt} + I_{dt} + I_r \qquad (20)$$

The values for each component can be found by multiplying our MétéoSuisse horizontal irradiance data by a "view factor" coefficient (Table 6), to account for panel slope. This process is detailed in sections II-B-5 through II-B-7.

Table 6
Liu & Jordan Isotropic Sky model. (Baldizon, 2019)

Liu & Jordan Isotropic Sky Model										
Gt	=	Gb	Rb	+	Gd	((1+cosβ)/2)	+	Gg	ρ	((1-cosβ)/2)
Total Incident Solar Irradiance on Tilted Surface		Beam Irradiance on Horizontal Surface	Beam View Factor		Diffuse Irradiance	Tilted Surface View Factor		Global Irradiance	Albedo	Tilted Surface View Factor
		Beam Component			Diffuse-Sky Component			Diffuse-Ground Component		

Note: "G" is interchangeable with "I" in referring to irradiance.

This model is isotropic, assuming equal intensity throughout the visible 'sky-dome'. Liu & Jordan's model does not account for an elevated intensity in diffuse radiation, such as horizon brightening or overcast skies. These factors are included in anisotropic models like the HDKR and Perez anisotropic models (Baldizon, 2019), both of which are more accurate, including location-specific empirical data in their estimate, but therefore more complex. For this investigation, Liu & Jordan's model was selected for its simplicity combined with the limited data provided by MétéoSuisse.

5. Tilted diffuse radiation

Tilted diffuse radiation is calculated as follows: (Maleki, Hizam, & Gomes, 2017)

$$I_{dt} = \left(\frac{1 + cos\beta}{2}\right) \times I_d$$

Using the MétéoSuisse reading for I_H at 11:00 on January 1st and an example slope angle of 45°:

$$I_{dt} = \left(\frac{1 + cos\,45}{2}\right) \times 171 \approx 146\; W\; m^{-2}$$

Note: the I_{dt} value will always be smaller than I_d; any tilt other than horizontal will eclipse some portion of the sky sphere from view, yielding a view tilt factor < 1.

Table 7
Sample horizontal diffuse and tilted diffuse irradiance from MétéoSuisse

Date + time	I_d (W·m^{-2})	I_{dt} (W·m^{-2})
1/1/15 08:00	34	29
1/1/15 09:00	78	67
1/1/15 10:00	103	88
1/1/15 11:00	171	146
1/1/15 12:00	158	135
1/1/15 13:00	114	97
1/1/15 14:00	93	79
1/1/15 15:00	33	28

6. Tilted beam irradiance

For tilted beam irradiance, the 'view factor' is replaced with a 'beam ratio' calculated, in this investigation, using the approach outlined by Duffie (Duffie & Beckman, p. 24). Beam ratio for a full day:

$$R_b = \frac{a}{b} = \frac{\omega_{ss} \sin\delta \sin(\phi - \beta) + \cos\delta \cos(\phi - \beta) \sin\omega_{ss}}{\omega_{sr} \sin\delta \sin\phi + \cos\delta \cos\phi \sin\omega_{sr}} \qquad (21)$$

Where ω_{sr} is the sunrise hour angle (the angle through which the Earth would turn to bring the meridian of the point directly under the sun) for an inclined surface, and ω_{ss} is the sunset hour angle. By convention, ω_{sr} is negative and ω_{ss} is positive; however, Eq. 22 requires both angles to be positive, $\omega_{sr} = \omega_{ss}$, such that:

$$R_b = \frac{a}{b} = \frac{\omega_{sr} \sin\delta \sin(\phi - \beta) + \cos\delta \cos(\phi - \beta) \sin\omega_{sr}}{\omega_{sr} \sin\delta \sin\phi + \cos\delta \cos\phi \sin\omega_{sr}} \quad (22)$$

The advantage of this method is that it takes into account the sunrise and sunset hours, providing an average only of hours when the panel is illuminated, and is simple to calculate in Excel.

The calculations for 11:00 Jan 1st are shown below (in radians), with ω_{sr} and declination angle δ calculated in Excel from literature equations (Kalogirou, p. 56):

$$R_b = \frac{1.113 \sin -0.4016 \ \sin(46.2044 - 45) + \cos -0.4016 \cos(46.2044 - 45) \sin 1.113}{1.113 \sin -0.4016 \sin 46.2044 + \cos -0.4016 \cos 46.2044 \sin 1.113}$$
$$\approx 1.458 = 145.8\%$$

And since $I_{bt} = R_b \times I_b$:

$$I_{bt} = R_b \times I_b = 1.458 \times 42 \approx 61 \ W \cdot m^{-2}$$

Table 8
Tilted Beam irradiance calculations using Duffie's R_b formula

Date + time	I_b (W·m^{-2})	ws	a	b	R_b daily (%)	$I_{b,t}$ (W·m^{-2})
1/1/15 08:00	1	1.11253	0.82527	0.56592	1.458273	1.5
1/1/15 09:00	2	1.11261	0.82533	0.56596	1.458271	2.9
1/1/15 10:00	1	1.11269	0.82538	0.56600	1.458270	1.5
1/1/15 11:00	42	1.11277	0.82543	0.56603	1.458268	61.2
1/1/15 12:00	109	1.11285	0.82548	0.56607	1.458266	159.0
1/1/15 13:00	143	1.11293	0.82554	0.56611	1.458264	208.5
1/1/15 14:00	66	1.11301	0.82559	0.56615	1.458262	96.2
1/1/15 15:00	33	1.11309	0.82565	0.56618	1.458261	48.1

7. Ground-reflected radiation

The calculation for ground-reflected radiation I_r (radiation reflected onto the panel from surfaces surrounding the panel location) (Eq. 23) features a similar view factor to I_{dt}, with the addition of a surface reflectivity (albedo) coefficient ρ, unique to this nearby ground:

$$I_r = I_H \rho \frac{1 - cos\beta}{2} \quad (23)$$

Given that concrete has an albedo of 0.2 (Marceau & VanGeem, 2008), the surface reflectivity was presumed a constant $\rho = 0.2$ (20%) throughout the year, as is standard practice (Maleki, Hizam, & Gomes, 2017). In reality, ρ will fluctuate according to meteorological conditions—however calculated I_r never exceeded 22 W·m^{-2} over the entire year, suggesting this was unlikely to have greatly skewed the data (global irradiance usually surpasses 200 W·m^{-2} daily.)

Table 9
Reflected irradiance calculations from MétéoSuisse data

Date + time	I_H (W·m^{-2})	Albedo p (%)	I_r (W·m^{-2})
1/1/15 08:00	35	0.2	1
1/1/15 09:00	80	0.2	2
1/1/15 10:00	104	0.2	3
1/1/15 11:00	213	0.2	6
1/1/15 12:00	267	0.2	8
1/1/15 13:00	257	0.2	8
1/1/15 14:00	159	0.2	5
1/1/15 15:00	66	0.2	2

For 11:00 January 1st :

$$I_r = 213 \times 0.2 \times \frac{1 - cos\, 45°}{2} \approx 6\, W \cdot m^{-2}$$

8. Finding total tilted irradiance from components

Finally, the tilted diffuse, beam, and reflected irradiation values can be summed as in equation 21 to find the hourly total tilted irradiance I_t :

$$I_t = I_{bt} + I_{dt} + I_r$$

For 11:00 January 1st :

$$I_t = 61 + 146 + 6 = 213\, W \cdot m^{-2}$$

Table 10
Total tilted irradiance calculations

Date + time	I_{dt} (W·m^{-2})	I_r (W·m^{-2})	I_{bt} (W·m^{-2})	I_t (W·m^{-2})
1/1/15 08:00	29	1	1.5	31.5
1/1/15 09:00	67	2	2.9	71.8
1/1/15 10:00	88	3	1.5	92.4
1/1/15 11:00	146	6	61.2	213.4
1/1/15 12:00	135	8	159.0	301.6
1/1/15 13:00	97	8	208.5	313.4
1/1/15 14:00	79	5	96.2	180.3
1/1/15 15:00	28	2	48.1	78.2

9. Finding energy output as a product of tilted irradiance and efficiency function

Now the hourly irradiance incident on the panel is known, it can be converted to power output P_{out} using the panel efficiency formula $\eta(\theta)$ as estimated in Section IIA, transforming equation 16 into equation 24 below:

$$P_{out} = I_t \times \eta(\theta) = I_t \times 0.01967 \times \cos(0.03107 \times \theta + 6.081) + 0.01516 \quad (24)$$

For 11:00 on Jan 1st:

Using Duffie's equation for the AOI (Eq. 1): $\theta \approx 28.25°$.

$$P_{out} = 213 \times 0.01967 \times \cos(0.03107 \times 28.25 + 6.081) + 0.01516$$
$$\ldots = 213 \times 0.03049 \approx 6.5\ W \cdot m^{-2}$$

Furthermore, because the data collection time interval used here was 1 hour, power (W) multiplied by time interval in hours (1h) will equal the output energy in Wh. Between 11:00 and 12:00, $P_{out} = 6.5\mathrm{W} \cdot \mathrm{m}^{-2} = 6.5\mathrm{Wh} = 23.4\mathrm{kJ}$.

Table 11
Sample output energy conversion

Date + time	I_t (W·m^{-2})	AOI (θ) (degrees)	Efficiency coefficient (%)	Output energy (Wh)
1/1/15 08:00	31.5	63.1	0.0115	0.4
1/1/15 09:00	71.8	50.0	0.0194	1.4
1/1/15 10:00	92.4	37.9	0.0262	2.4
1/1/15 11:00	213.4	28.2	0.0305	6.5
1/1/15 12:00	301.6	24.2	0.0319	9.6
1/1/15 13:00	313.4	28.2	0.0305	9.6
1/1/15 14:00	180.3	37.9	0.0262	4.7
1/1/15 15:00	78.2	50.0	0.0194	1.5

Table 11 presents a sample of hourly output energy data. Figure 12 below shows a 3D scatterplot of the total output energy (Wh) for every day of the year, for every slope angle from 0°- 90° in 5° increments. The 6570 datapoints are color-coded by output energy.

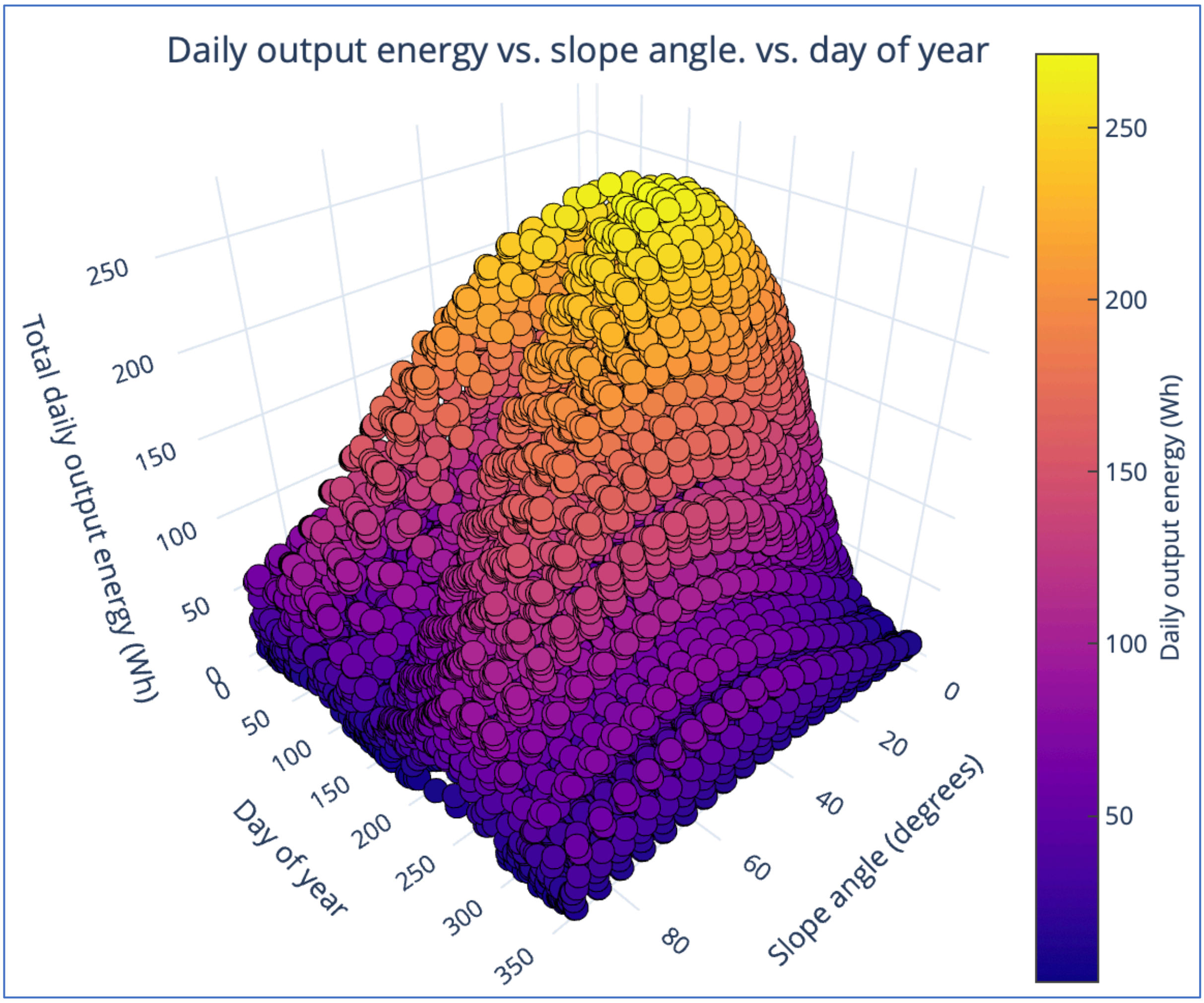

Figure 12. Daily output energy vs. Slope angle vs. Day of year, Plotted in Plot.ly

Slope angles from ~90°-45° produce dual peaks along the day axis (seen as ridges on the plot), indicating maximum outputs in spring and autumn for $\beta \gg 45°$. Conversely, $\beta \lesssim 45°$ shows a single, increasingly steep peak during summer (Day=~180). The peak daily output is found in June for β=40°.

10. Integrating output energy over a full year

The value for energy (Wh) produced every hour over a full year can be integrated with respect to time (interval t_h=1 h), thereby summing the annual energy produced (Al-Haidari, 2017):

$$E_{out,year} = \sum_{j=1}^{365} \int_{sr}^{ss} P_{out}\, dt_h \qquad (25)$$

where *sr* is the sunrise time, *ss* is the sunset time. This calculation was performed using the Excel SUM function, excluding all values outside of the *sr* to *ss* range, to find the total annual output energy at a given angle.

The slope angle was then varied in 5° increments and $E_{out,year}$ recorded (Table 12).

Table 12
Total annual energy output at different panel slope angles

Panel slope angle (°)	$E_{out,year}$ $(Wh \cdot m^{-2})$
0	23962
5	27227
10	30262
15	32953
20	35208
25	36966
30	38209
35	38879
40	38953
45	38405
50	37246
55	35512
60	33260
65	30568
70	27543
75	24302
80	20933
85	17548
90	14270

C. Optimization, results and analysis

1. Slope angle optimization

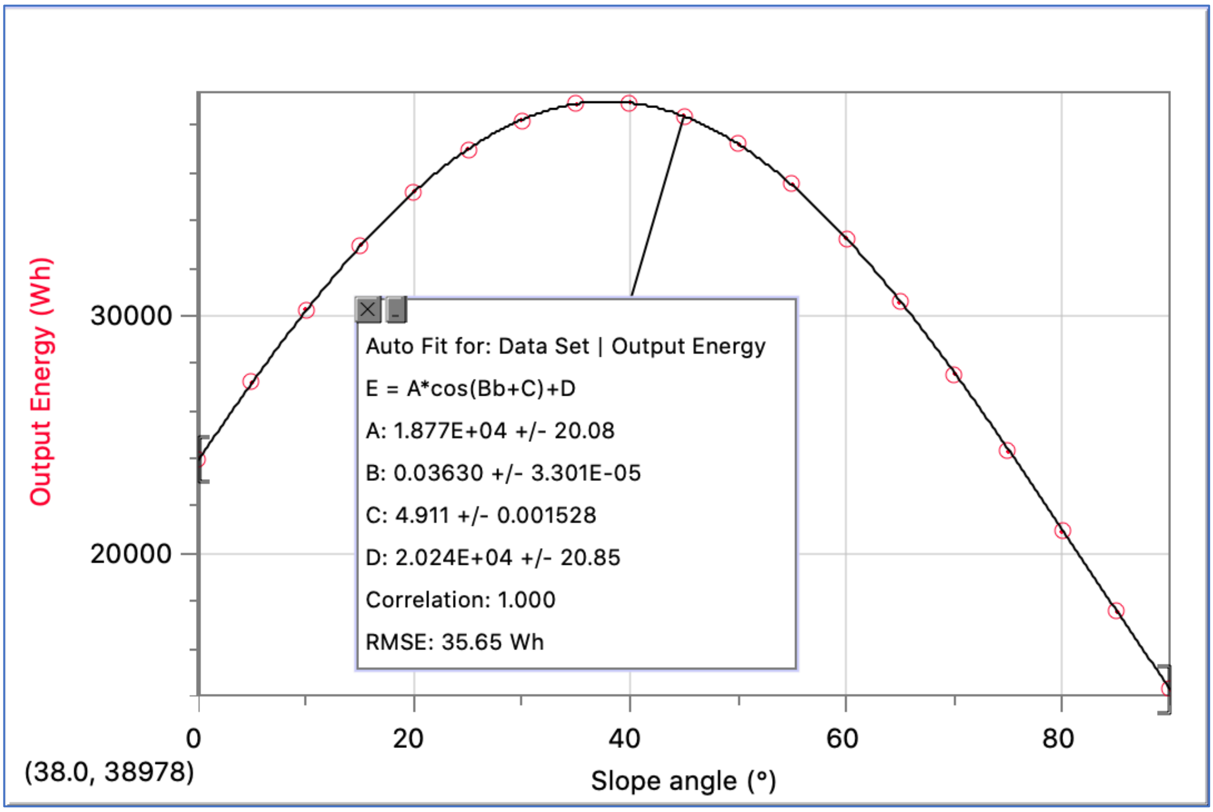

Figure 13. Optimization of annual slope angle for maximum energy output, plotted in LoggerPro

Figure 13 graphs the values from Table 12 for total annual output energy vs. slope angle. A sinusoidal regression line (arising from the data being angle-related) shows a maximum of 38’978 Wh at a slope angle of 38.0°. This demonstrates that a solar panel tilted at the optimum slope angle of 38.0° for maximum output energy generation in Geneva, Switzerland will gain around 895 Wh·m^{-2} (3.22 MJ·m^{-2}) annually over a panel positioned according to Geneva’s latitude (46.2°N).

2. Optimum slope angle at intervals

This optimization approach can be extended for time intervals other than annual (while remaining in a fixed position over a given interval). Many large-scale solar installations have workers manually adjusting panel position several times a year to maximize energy. Increased frequency of adjustments—annual (E_A), semi-annual (E_{S1}, E_{S2}), seasonal (E_{Q1} … E_{Q4}), monthly—will result in higher annual outputs with decreasing interval granularities, as intervals tend towards real-time solar tracking like that employed on HVATs and DATs (Khorasanizadeh, Mohammadi, & Mostafaeipour, 2014).

To find these values: For each angle (in 5° increments from 0°-90°, and 10° increments from 90°-120°) the output energy is found for each month of the year. For seasonal/semi-annual/annual intervals, energy output is calculated as the sum of the corresponding months as shown in the equations below, then plotted in an optimization graph (Figure 14).

$$E_{Q1} = \sum E_{Jan} + E_{Feb} + E_{Mar} \qquad E_{S1} = \sum E_{Apr} + E_{May} + \cdots + E_{Sep}$$

$$E_{Q2} = \sum E_{Apr} + E_{May} + E_{Jun} \qquad E_{S2} = \sum E_{Oct} + E_{Nov} + \cdots + E_{Mar}$$

$$E_{Q3} = \sum E_{Jul} + E_{Aug} + E_{Sep}$$

$$E_{Q4} = \sum E_{Oct} + E_{Nov} + E_{Dec} \qquad E_{A} = \sum E_{Jan} + E_{Feb} + \cdots + E_{Dec}$$

Note: the semi-annual interval is split between September and October, not June and July, to better reflect Geneva's 'wintertime' from October to March and 'summertime' from April to September.

Table 13
Output energy at different angles for each interval

	Monthly												Seasonal				Semi-annual		Annual
angle	Jan	Feb	Mar	Apr	May	Jun	Jul	Aug	Sep	Oct	Nov	Dec	Q1	Q2	Q3	Q4	S1	S2	A
0	222	511	1681	2791	2670	3938	4598	3900	2286	949	253	164	2414	9399	10784	1366	20183	3780	23962
5	316	654	2017	3176	2878	4246	5046	4403	2700	1201	349	241	2988	10300	12149	1791	22449	4778	27227
10	418	802	2349	3532	3046	4495	5426	4858	3100	1460	451	326	3569	11072	13384	2237	24456	5806	30262
15	524	949	2664	3844	3168	4673	5722	5248	3473	1719	555	414	4136	11686	14443	2688	26129	6825	32953
20	630	1089	2951	4101	3242	4777	5925	5559	3805	1967	658	504	4670	12121	15289	3128	27410	7798	35208
25	732	1219	3200	4295	3267	4816	6035	5781	4082	2194	756	590	5150	12378	15897	3541	28275	8691	36966
30	827	1332	3401	4420	3252	4792	6070	5909	4295	2393	847	672	5560	12464	16274	3911	28738	9471	38209
35	911	1426	3547	4477	3198	4689	6011	5956	4439	2555	925	744	5884	12364	16406	4225	28769	10109	38879
40	982	1497	3635	4474	3097	4513	5853	5921	4509	2676	990	806	6114	12084	16283	4472	28367	10586	38953
45	1037	1542	3665	4409	2947	4262	5593	5789	4517	2752	1038	854	6244	11618	15899	4644	27517	10888	38405
50	1073	1562	3645	4272	2754	3942	5239	5558	4464	2781	1068	888	6281	10969	15260	4737	26228	11018	37246
55	1092	1557	3577	4065	2523	3567	4802	5234	4342	2767	1081	906	6225	10155	14378	4754	24532	10979	35512
60	1091	1530	3455	3793	2262	3149	4299	4829	4149	2719	1075	908	6077	9204	13277	4702	22481	10779	33260
65	1073	1486	3279	3467	1980	2704	3749	4357	3890	2633	1054	895	5838	8151	11996	4582	20148	10420	30568
70	1043	1421	3053	3098	1687	2256	3176	3836	3575	2506	1021	870	5517	7041	10587	4397	17628	9915	27543
75	1001	1336	2787	2701	1397	1818	2609	3286	3214	2341	975	838	5124	5915	9109	4154	15024	9278	24302
80	944	1234	2488	2289	1117	1398	2058	2731	2821	2144	916	794	4666	4803	7610	3854	12413	8520	20933
85	875	1117	2169	1879	852	1010	1540	2190	2411	1921	845	739	4160	3742	6141	3505	9883	7666	17548
90	796	989	1840	1485	612	675	1073	1680	1999	1681	764	675	3625	2772	4752	3121	7524	6746	14270
100	616	721	1203	794	237	184	368	812	1228	1186	586	529	2540	1215	2407	2301	3622	4841	8463
110	430	466	658	292	28	0	17	232	604	728	405	376	1555	320	853	1509	1172	3064	4236
120	262	255	265	31	0	0	0	7	188	364	245	235	782	31	195	844	226	1626	1852
Slope opt	**60**	**53**	**46**	**37.1**	**26**	**25**	**28.6**	**34.7**	**43.3**	**52.2**	**58.2**	**60.1**	**50.1**	**29.5**	**34.7**	**55.1**	**32.5**	**52.4**	**38**
Eout opt	**1095**	**1569**	**3682**	**4508**	**3286**	**4848**	**6107**	**5993**	**4542**	**2795**	**1083**	**908**	**6299**	**12518**	**16451**	**4779**	**28929**	**11063**	**38993**

Table 13 displays the output energy for each interval for each angle, enabling optimization curves like Figures 13 (above) and 14 (below) to be plotted, finding the optimal angle using a sinusoidal regression line as shown for the example of January (E_{Jan}) below.

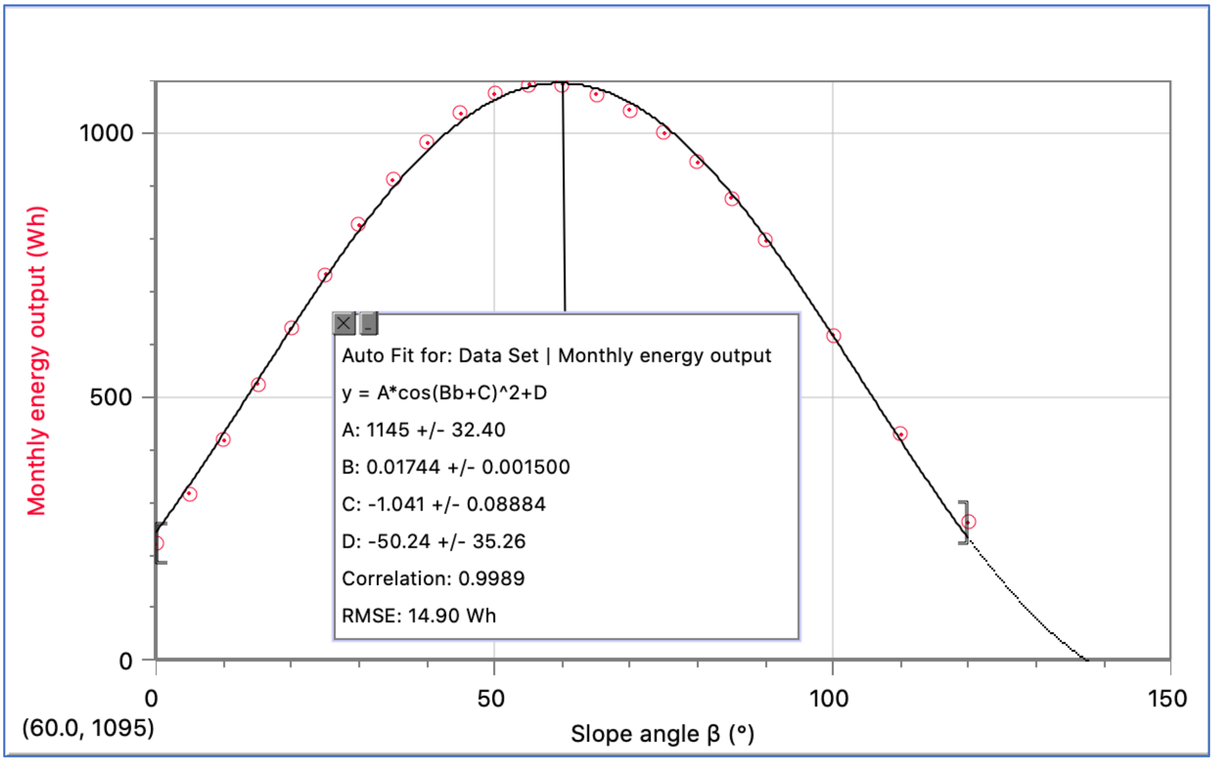

Figure 14. Slope optimization curve for total energy generation in January

The optimal slope angles at different time intervals are summarized in Table 14 below (colored by interval):

Table 14
Optimum panel slopes over a year at different intervals

Month	Monthly	Seasonal	Semi-annual	Annual
January	60.0	50.1	52.4	38.0
February	53.0	50.1	52.4	38.0
March	46.0	50.1	52.4	38.0
April	37.1	29.5	32.5	38.0
May	26.0	29.5	32.5	38.0
June	25.0	29.5	32.5	38.0
July	28.6	34.7	32.5	38.0
August	34.7	34.7	32.5	38.0
September	43.3	34.7	32.5	38.0
October	52.2	55.1	52.4	38.0
November	58.2	55.1	52.4	38.0
December	60.1	55.1	52.4	38.0

And the data can be plotted over the course of a year (Figure 15):

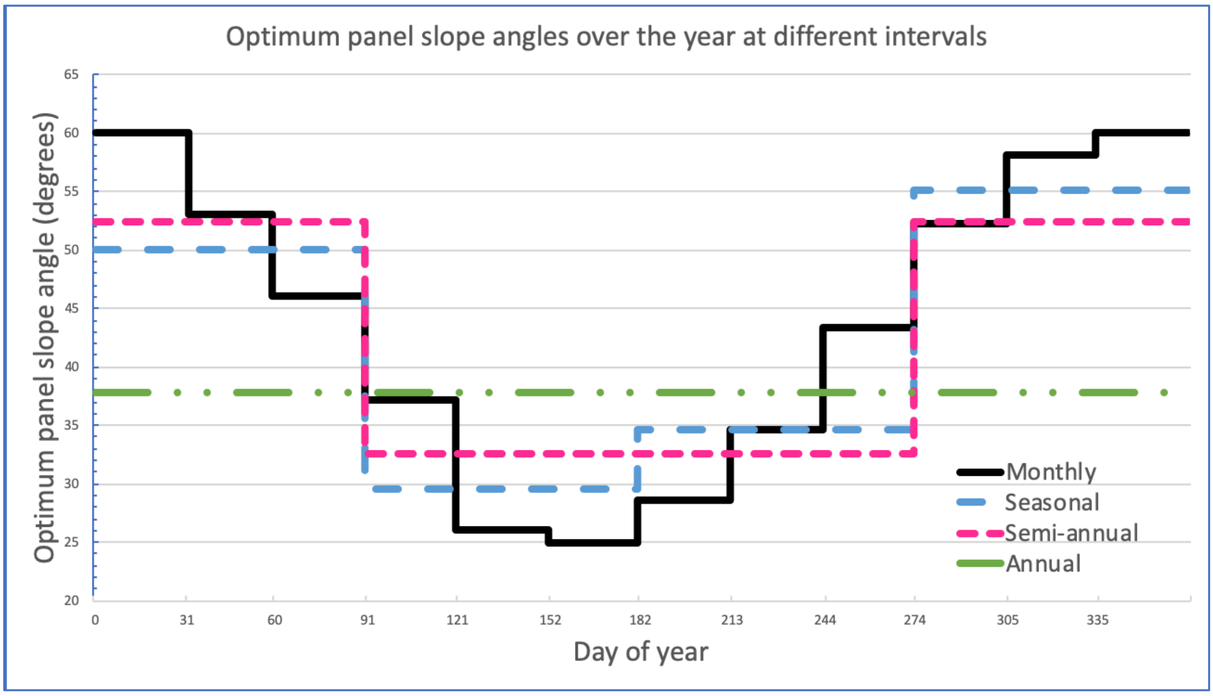

Figure 15. Optimum panel slope angles over the year at different intervals, plotted in Excel

The semi-annual adjustment optimal slopes (52.4°/32.5°) differ from the hypothesized $\phi \pm 15°$ by 8.8° and 1.3° respectively, meaning that the wintertime half-year diverges more from the model. Interestingly, the E_{S1} winter months were observed to have lower correlation coefficients when plotting optimization curves. This unpredictability may perhaps arise from Switzerland's precipitation-heavy winters, compared to similar latitudes.

The utility of this interval comparison lies in a cost-benefit relationship between the human effort required to manually adjust panels at increasingly short intervals, and the benefit of increased energy output:

Table 15
Comparison of tilt adjustment intervals for output energy generation

Tilt Adjustment Interval	Energy out ($Wh{\cdot}m^{-2}$)	Improvement from horizontal ($Wh{\cdot}m^{-2}$)	Improvement from horizontal (%)	Improvement from horizontal: change from prev. improvement (%)
12x / year (monthly)	40416	16454	68.7	1.5
4x / year (seasonally)	40047	16085	67.1	0.2
2x / year (semi-annually)	39992	16030	66.9	4.2
1x / year (annually)	38993	15031	62.7	62.7
0x / year (permanently horizontal)	23962	0	0.0	0.0

The largest single improvement lies between a horizontal panel and an optimally tilted annual setup, seeing an energy output gain of 15 kWh annually. The conversion to semi-annual adjustments makes the second largest difference, with an energy increase of 4.2%. Shifting from semi-annual to seasonal is only a 0.2% increase, and monthly only another 1.5%; changing to seasonal is the least worthwhile, with monthly a close second, considering that the monthly interval would entail six times as many adjustments than the semi-annual interval.

For most purposes the annual interval with a fixed panel slope of 38.0° is adequate, while use cases with sufficient manpower and/or the need for as much energy as possible, would benefit from a semi-annual setup to gain an additional 4.2% energy annually.

III. Conclusion

This paper investigates southern-facing polycrystalline PV panel performance in Geneva, Switzerland using MétéoSuisse typical meteorological year data [2010-2019]. Annual tilted insolation was estimated using the Liu & Jordan isotropic model and optimized for maximum output at a range of adjustment intervals.

The optimum slope angle for an annual adjustment frequency was identified as 38.0°, given an azimuth angle of 0°N. This differs from Geneva's latitude (46.2°N) by 8.2°, demonstrating limitations of the '$\beta_{opt} = \phi$' convention.

Under reasonable assumptions, the most beneficial adjustment interval (other than annual-tilted) was found to be semi-annual, with diminishing returns from seasonal and monthly adjustments. The semi-annual optimum slope angles (52.4°/32.5°) differed from the convention ($\phi + 15° = 61.2°$, $\phi - 15° = 31.2°$) by 8.8° (winter) and 1.3° (summer), exemplifying the need for location-specific optimum-angle investigations.

There are limitations to the investigation methodology, however. The panel used in Section A was found to have a maximum 3.3% efficiency, whereas commercial panels have efficiencies of 18% (Which Solar Panel Type is Best?, 2013), suggesting weaknesses in the laboratory testing method or apparatus. The use of a typical meteorological year is, ultimately, historical. Trends like climate change make the meteorological future increasingly unpredictable, possibly rendering these investigation results short-lived.

An extension of this model could optimize the panel azimuth in addition to the slope, supplementing the Liu & Jordan model with the KT method, as demonstrated by Yan et al. (2013). Alternatively, an investigation may be worth pursuing into optimizing panel slope for maximum profit generation on the grid, as shown by Rowlands et al. (2011).

IV. Works Cited

Al-Haidari, S. (2017). *A look at the optimum tilt angle of a fixed solar panel for maximum energy collection for a one year time frame - Thesis submitted for Master of Science in Mechanical Engineering.* Babylon, Iraq: Wright State University / University of Babylon, Iraq.

Allen, J. (2018, November 30). *Tilt & Azimuth Angle: Finding the Optimal Angle to Mount Your Solar Panels*. Retrieved from Wholesale Solar: https://www.wholesalesolar.com/blog/solar-panel-azimuth-angle/

Bakirci, K. (2012). General models for optimum tilt angles of solar panels: Turkey case study. *Renewable and Sustainable Energy Reviews*, 6149–6159.

Baldizon, R. (2019, May 15). *What are Sky Models?* Retrieved from Medium / Luszol Solar: https://medium.com/luszol/what-are-sky-models-40fac8c5d4ba

Benghanem, M. (2011). Optimization of tilt angle for solar panel: Case study for Madinah, Saudi Arabia. *Applied Energy*, 1427–1433.

Berisha, X., Zeqiri, A., & Meha, D. (2018). Solar Radiation–The Estimation of the Optimum Tilt Angles for South-Facing Surfaces in Pristina. *International Journal of Recent Advancement in Engineering and Research*, 7-19.

Bond, M. (n.d.). *Solar power plant in the Alps, Switzerland.* Science Photo Library.

CircuitGlobe. (2018, February 16). *Photovoltaic Solar Cell Basics*. Retrieved from CircuitGlobe.com: https://circuitglobe.com/photovoltaic-or-solar-cell.html

Duffie, J. A., & Beckman, W. A. (2013). Solar Engineering of Thermal Processes. Solar Energy Laboratory University of Wisconsin-Madison.

Elminir, H. K., Ghitas, A. E., El-Hussainy, F., Hamid, R., Beheary, M., & Abdel-Moneim, K. M. (2006). Optimum solar flat-plate collector slope: Case study for Helwan, Egypt. *Energy Conversion and Management*, 624–637.

Federal Office of Topology. (2017, November 27). *Geography – Facts and Figures*. Retrieved from Admin.ch - Confédération Suisse: https://www.eda.admin.ch/aboutswitzerland/en/home/umwelt/geografie/geografie---fakten-und-zahlen.html

IEC IECEE. (2005, December 8). *IEC 60950-1:2005*. Retrieved from IEC System of Conformity Assessment Schemes for Electrotechnical Equipment and Components: https://webstore.iec.ch/preview/info_iec60950-1%7Bed2.0%7Den_d.pdf

ISE. (2019). *Photovoltaics Report.* Freiburg: Fraunhofer Institute for Solar Energy Systems, ISE. Retrieved from https://www.ise.fraunhofer.de/content/dam/ise/de/documents/publications/studies/Photovoltaics-Report.pdf

Kalogirou, S. A. (2014). *Solar Engineering Systems.* Academic Press - Elsevier.

Khorasanizadeh, H., Mohammadi, K., & Mostafaeipour, A. (2014). Establishing a diffuse solar radiation model for determining the optimum tilt angle of solar surfaces in Tabass, Iran. *Energy Conversion and Management*, 810-811.

LeNews. (2019, May 31). *Switzerland ranks near bottom for solar and wind energy*. Retrieved from LeNews.ch: https://lenews.ch/2019/05/31/switzerland-ranks-near-bottom-for-solar-and-wind-energy/

Maleki, S. A., Hizam, H., & Gomes, C. (2017). Estimation of Hourly, Daily and Monthly Global Solar Radiation on Inclined Surfaces: Models Re-Visited. *Energies*, 134-162.

Marceau, M. L., & VanGeem, M. G. (2008). *Solar reflectance values of concrete.* Skokie, Illinois: Portland Cement Association.

MétéoSuisse. (2015, June). *Désignation de la qualité des valeurs mesurées.* Retrieved from Federal Office of Meteorology and Climatology MeteoSwiss: https://gate.meteoswiss.ch/idaweb/text/datenqualitaet_legende_fr.pdf

Mohammadi, K., Mostafaeipour, A., & Khorasanizadeh, H. (2014). Establishing a diffuse solar radiation model for determining the optimum tilt angle of solar surfaces in Tabass, Iran. *Energy Conversion and Management*, 805-814.

Office of Energy Efficiency & Renewable Energy. (2017, October 12). *onfronting the Duck Curve: How to Address Over-Generation of Solar Energy*. Retrieved from Office of Energy Efficiency & Renewable Energy: https://www.energy.gov/eere/articles/confronting-duck-curve-how-address-over-generation-solar-energy

OSRAM. (2007, May 10). *OSRAM FCS 64640 150W 24V HLX Halogen Light Bulb*. Retrieved from Amazon.com: https://www.amazon.com/OSRAM-64640-150W-Halogen-Light/dp/B000QHADQI

Rezrazi, A., Laidi, M., & Hanini, S. (n.d.). An optimisation methodology of artificial neural network models for predicting solar radiation: a case study. *Theoretical and Applied Climatology.* Dr. Yahia Fares University of Médéa, Saad Dahlab University.

Rowlands, I. H., Kemery, B. P., & Beausoleil-Morrison, I. (2011). Optimal solar-PV tilt angle and azimuth: An Ontario (Canada) case-study. *Energy Policy*, 1397-1409.

Solar Calculator. (2015, December 15). *The effect of temperature on solar panel performance*. Retrieved from Solar calculator: https://solarcalculator.com.au/solar-panel-temperature/

Solar technologies office. (2013, August 20). *Solar Performance and Efficiency* . Retrieved from Office of energy efficiency & renewable energy: https://www.energy.gov/eere/solar/articles/solar-performance-and-efficiency

The National Renewable Energy Laboratory (NREL). (2019, May 29). *Solar Resource Glossary*. Retrieved from NREL.gov: https://www.nrel.gov/grid/solar-resource/solar-glossary.html#radiation

Weik, M. H. (2001). Lambert's cosine law. In *Computer Science and Communications Dictionary* (pp. 868-868). Boston, MA: Springer US.

Westin, S. H. (2011, September 5). *Fresnel Reflectance*. Retrieved from Cornell University Graphics Department: http://www.graphics.cornell.edu/~westin/misc/fresnel.html

Which Solar Panel Type is Best? (2013, June). Retrieved from Energy Informative: https://energyinformative.org/best-solar-panel-monocrystalline-polycrystalline-thin-film/

Yan, R., Saha, T. K., Meredith, P., & Goodwin, S. (2013). Analysis of yearlong performance of differently tilted photovoltaic systems in Brisbane, Australia. *Energy Conversion and Management*, 102–108.

V. APPENDIX

Note: Raw data tables are not provided for this investigation, due to insufficient space; meteorological data comprises 8760 rows and over 200 columns in order to produce the graphs shown. Instead, table samples have been provided throughout the body text, where relevant. Raw horizontal irradiance data is available from the MétéoSuisse IDAWEB portal, after a brief access-request process. In addition the collection of (Macro-enabled) Excel Spreadsheets used are provided at this web address:

https://app.blackhole.run/#0wrKfcE01i14ChWZmo9E9GLvHLExhEdSZ6BdzKNnf4Wq